Correlation-engineered dynamic phases in wax-based soft matter observed via optical speckle analysis

Tatiana Meshkova
Qufit B.V., Netherlands

December 2025

Abstract

We report reproducible differences in dynamical correlation structure that can persist in condensed media beyond what is captured by chemical composition alone.

As an experimental realization, we report a correlation-structured dynamical state (CCIM-DP)—used here as a descriptive label for the observed phenomenology—in a wax-based condensed medium subject to disclosure constraints on processing details.

Using time-resolved optical speckle analysis (power spectral density, two-dimensional spatial autocorrelation, temporal autocorrelation, phase-locking value, anisotropy, and effective correlation length), we observe extended spatial correlations, multiscale temporal organization, and partial phase synchronization in structured specimens that are absent in chemically identical controls.

In the specific implementation reported here, the material dynamics are aligned with a reference fluctuation template derived from optical speckle measurements of an aqueous reference system. The reference is used solely as an instrumentally measurable fluctuation template; no biological, pharmacological, or therapeutic implication is made.

The results demonstrate that a prescribed fluctuation-statistics template can be used to specify target correlation features in a chemically distinct soft condensed medium without material transfer, establishing a reproducible experimental route toward correlation-engineered dynamical states in soft matter.

Keywords: soft condensed matter; non-equilibrium dynamics; correlation-structured dynamics; optical speckle analysis; dynamical correlation order; mesoscopic coherence; phase synchronization; Kuramoto-type models; time-resolved speckle statistics; phase-locking value; power spectral density.

1 Introduction: Correlation-structured dynamical states

Modern condensed-matter physics explains a wide range of equilibrium and non-equilibrium phenomena through interactions, symmetry breaking, and energetic considerations. However, many complex systems exhibit persistent collective dynamics, long-range correlations, reproducible functional behaviour, and strong dependence on formation history that cannot be fully reduced to static structure or chemical composition [1, 2].

We adopt a correlation-centered descriptive approach in which matter is characterized not only by its constituents, but by the architecture of dynamical correlations linking internal degrees of freedom across space and time. Within this approach, correlation order is treated as an organizing descriptor capable of defining stable, reproducible dynamical states.

Conceptual framing and contribution boundary. In the present paper, this framing is used strictly as an operational way to organize and interpret experimentally measured correlation observables. Correlation order is defined and evaluated via directly measurable statistical observables extracted from speckle dynamics [7, 8].

Scope of the present work (first experimental report). The present article is intended as a first experimental report. Its goal is to document an instrumentally measurable distinction between structured and non-structured specimens prepared from the same chemical matrix, using a specified optical acquisition and analysis pipeline and objective exclusion criteria. Comprehensive exploration of parameter space, extended replication across batches, and independent laboratory studies are reserved for subsequent work.

Reference system used in this study. As a concrete reference fluctuation template, we use an optical speckle recording of an aqueous reference solution as a physically stable, instrumentally measurable reference system for template-alignment of fluctuation statistics (Sec. 4.2). This reference is used solely in an optical measurement context and carries no biological, pharmacological, or therapeutic implication.

2 Correlation Order as a Practical Descriptor

Correlation order refers to structured phase relationships within an ensemble of interacting microdynamic elements. Unlike equilibrium order parameters, correlation order is inherently dynamical and can be characterized by:

- extended spatial correlations,
- multiscale temporal organization,
- partial phase synchronization,
- robustness to perturbations and handling.

When stabilized, correlation order can act as a practically useful descriptor for distinguishing dynamical states even in chemically identical materials.

3 Multiscale phenomenological framework

CCIM-DP can be described using a three-level framework combining Floquet-modulated oscillator ensembles, mesoscopic collective fields, and macroscopic correlation-energy minimization [3, 4, 5].

3.1 Microscopic Level: Floquet-Modulated Phase Dynamics

Let the material contain N weakly nonlinear oscillatory modes with phases $\theta_i(t)$. The dynamics follow a Floquet-modulated Kuramoto-type equation:

$$\dot{\theta}_i = \omega_i + \sum_{j=1}^{N} \Big[K_{ij}^{(0)} + \varepsilon\, F_{ij}(\xi(t)) \Big] \sin(\theta_j - \theta_i), \tag{1}$$

where ω_i are natural frequencies, $K_{ij}^{(0)}$ baseline couplings, $\xi(t)$ the reference fluctuation profile, and F_{ij} a functional describing template-induced modulation of effective couplings.

A convenient coherence descriptor is the Kuramoto order parameter:

$$r(t)e^{i\psi(t)} = \frac{1}{N}\sum_{j=1}^{N} e^{i\theta_j(t)}, \qquad r(t) \in [0,1],$$

where $r(t)$ measures instantaneous phase coherence.

3.2 Mesoscopic Level: Collective Field Dynamics

Define a collective oscillatory field

$$A(t) = \sum_{i=1}^{N} a_i e^{i\theta_i(t)}.$$

Its dynamics are described by a phenomenological Landau–Stuart (Fröhlich-type) amplitude equation [6]:

$$\dot{A} = (\mu - \gamma|A|^2)A + \eta(t) + \lambda S(t), \tag{2}$$

where μ and γ are effective gain/saturation parameters, $\eta(t)$ denotes stochastic fluctuations, and $S(t)$ is a structured input derived from the reference fluctuation template.

3.3 Macroscopic Level: Correlation-Energy Functional

The system minimizes an effective correlation functional

$$E_{\text{corr}} = -\sum_{ij} K_{ij}(t)\cos(\theta_i - \theta_j), \tag{3}$$

leading to self-organization into a stable correlation-structured dynamical state.

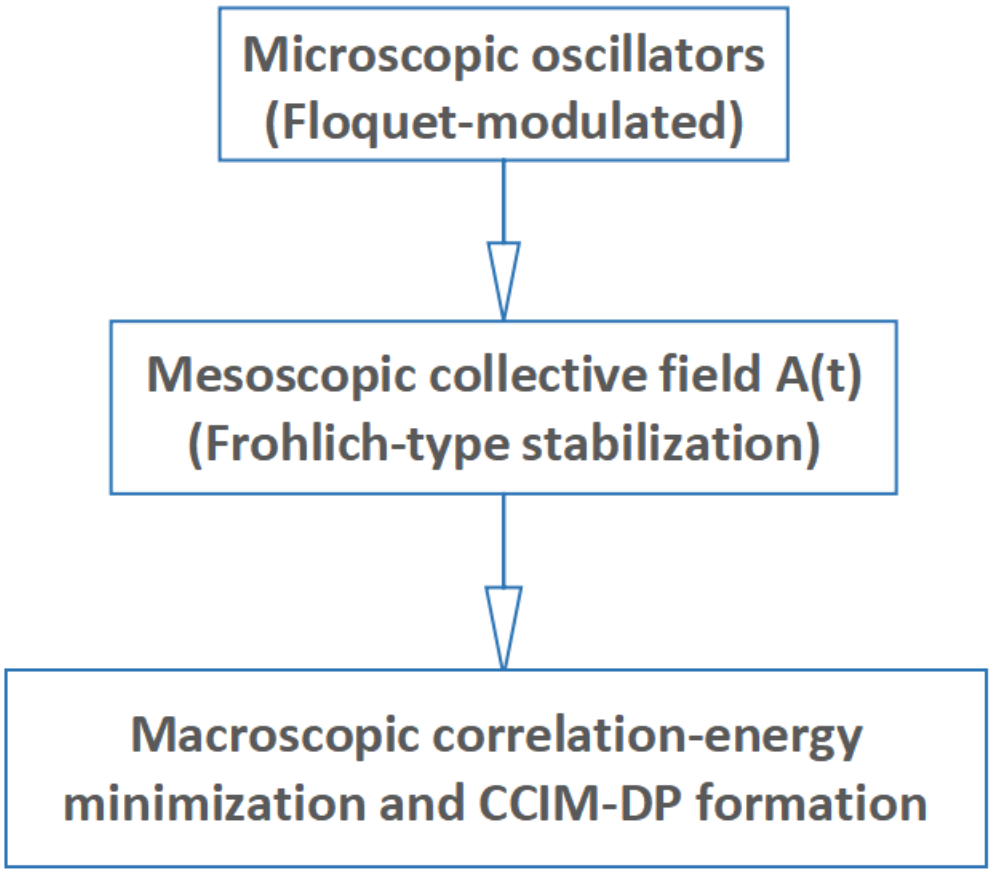

Figure 1: Schematic representation of correlation-structured dynamical state formation (CCIM-DP) in a wax-based soft condensed medium. Microscopic Floquet-modulated oscillator dynamics give rise to mesoscopic collective fields, which stabilize into a macroscopic correlation-structured regime characterized by extended spatiotemporal coherence.

4 Experimental System

4.1 Material Platform and Sampling

The studied system is a wax-based condensed medium. Two conditions were examined:

- **Structured (CCIM-DP):** material subjected to a structuring procedure to establish a target correlation architecture,
- **Control:** chemically identical material from the same batch without conditioning.

From a larger batch (approximately ten sticks per condition), $n = 3$ sticks per condition were randomly selected for the quantitative analysis reported here. Multiple videos were acquired per stick (Sec. 5.2), and multiple ROIs were evaluated per video (Sec. 5.3). Representative figures show one structured and one control instance, while distributions aggregate across the analyzed set.

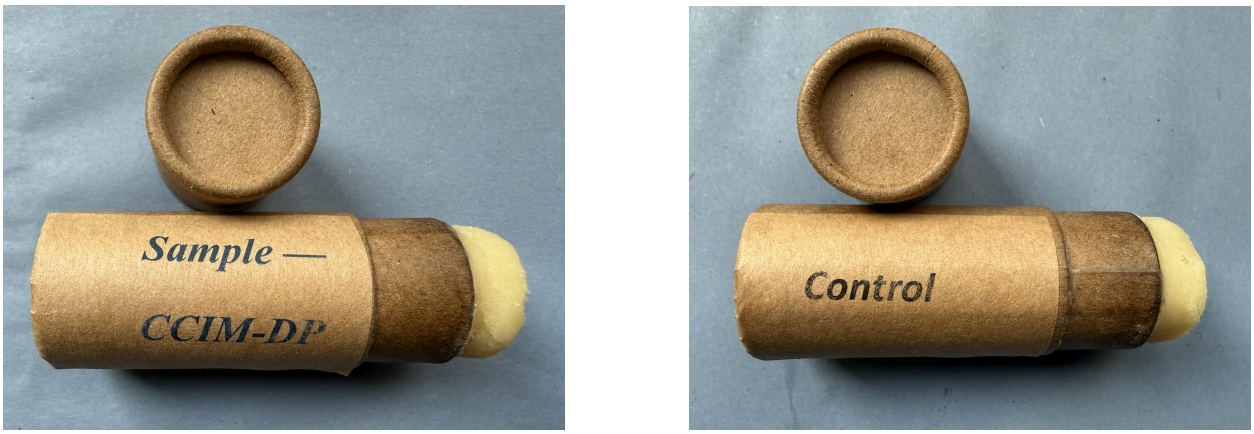

Figure 2: Representative photographs of the structured specimen (CCIM-DP, left) and the chemically identical control specimen (right) prepared from the same production batch and subjected to identical handling conditions, differing only by the application of the structuring step.

4.2 Correlation-structured state formation

The structuring procedure establishes and stabilizes a target correlation architecture in the material.

Reference used in this implementation (measurement-only). In this study, a reference fluctuation profile was extracted from the optical speckle signal of an aqueous *semaglutide* solution. Semaglutide is used here solely as a specific instance of a physically stable reference system with an instrumentally measurable fluctuation structure used for template-alignment of fluctuation statistics. This choice does not imply any biological, pharmacological, or therapeutic relevance; no functional or biochemical properties are transferred or inferred, and no reference material is introduced into the wax matrix at any stage.

Minimal protocol disclosure (reproducibility envelope). A semi-solid matrix from a single production batch was split into two portions: one portion was structured, while the other portion from the same batch was kept non-structured and served as the Control. Both portions were handled identically with respect to containers, ambient conditions, and waiting times; the only difference was the application (or absence) of the active structuring step. No material was added to either portion at any stage.

In this implementation, structuring was performed as a non-chemical conditioning step based on externally applied, time-varying physical stimulation whose target statistics were specified by the reference fluctuation template. The procedure was carried out at room temperature (21–24°C) for a fixed conditioning time T_{cond} (30–40 min in this series), followed by a fixed stabilization time T_{stab} (2–6 h in this series) prior to optical measurements.

To verify robustness under typical technological handling, the structured matrix was subjected to repeated melting/cooling/moulding cycles before measurements; in addition, a subset of the structured matrix was transferred to an independent laboratory and incorporated at approximately 25% by weight into a finished formulation using standard melting, mixing, casting, and cooling steps. Structured and control finished products (same batch, same formulation and processing) were analyzed in parallel by speckle-based dynamic scattering.

Table 1: Structuring protocol: minimal reproducibility parameters.

Parameter	Value / description
Batching	Single production batch; split into structured vs control portions
Active step	Non-chemical conditioning via externally applied time-varying physical stimulation
Conditioning time T_{cond}	30–40 min (fixed within series)
Stabilization time T_{stab}	2–6 h (fixed within series)
Ambient temperature	21–24°C
Handling parity	Identical containers/conditions/timelines; control without active step
Material addition	None (no additives introduced)
Robustness check	Repeated melting/cooling/moulding cycles prior to measurement
Inter-lab check	Transfer to independent lab; ∼25% w/w incorporation into final formulation

4.3 Generality of the Reference

The correlation-templating approach is not specific to semaglutide. Any system exhibiting reproducible speckle dynamics and coherent fluctuation structure can serve as a reference template. Semaglutide represents only one illustrative example.

5 Measurement Methods

5.1 Optical setup and geometry

Speckle dynamics were recorded under coherent CW laser illumination in a backscattering configuration. The illumination was incident at 10–20° relative to the surface normal, while the camera axis was aligned close to the normal. Typical distances were: laser–sample 15–30 cm; camera–sample 20–40 cm. No diffuser was used. A neutral-density (ND) filter was applied when needed to keep peak pixel values below $\sim 70\%$ of the camera dynamic range.

5.2 Acquisition hardware and camera settings

All speckle videos were recorded using an iPhone 16 Pro Max rigidly mounted on a tripod (no handheld acquisition). Focus and exposure were fixed prior to recording to avoid automatic adaptation artifacts.

Camera format and frame rate. The iPhone camera was configured as follows (iOS Settings → Camera): Formats: Most Compatible (H.264); Record Video: 1080p at 30 fps; Auto FPS (Low Light): OFF; HDR Video: OFF; Macro Control: OFF; View Outside the Frame: OFF; Preserve Settings: Camera Mode ON. In the Camera app, recordings were made at 1× zoom (no lens switching), without styles/filters.

Fixed focus and exposure. Immediately before each recording, AE/AF Lock was enabled by a long press in the Camera app to prevent autofocus and autoexposure adaptation during acquisition. A small negative exposure compensation was applied (typically -0.3 to -0.7 EV) to avoid clipping, overexposure, and visible flicker under coherent illumination. The nominal exposure time range was 1/60–1/120 s.

Environmental conditions and vibration control. All recordings were performed at room temperature (21–24°C). Vibration control was passive: a heavy table and damping material under the tripod; the camera and laser were not moved during a recording.

Acquisition duration and repeats. Each recording was 60–120 s. For each physical specimen, five recordings were acquired under identical settings, and multiple fixed-size ROIs were analyzed per recording using the same processing pipeline.

5.3 ROI selection and preprocessing

Regions of interest (ROI) of fixed size (256×256 to 512×512 px) were selected from the central area of the frame, avoiding borders and visible specular highlights. A highlight mask was used to exclude saturated/near-saturated pixels. A linear detrend (1st order) was applied to the ROI intensity time series.

Frame-drift estimation and exclusion criterion. Frame-to-frame displacement was estimated via phase correlation (Fourier cross-correlation) on the central ROI with Gaussian prefilter $\sigma = 1.2$; recordings with median displacement > 0.2 px/frame (or P95 > 0.5 px/frame) were excluded.

Validation against iOS OIS/EIS artifacts. To validate OIS/EIS, we recorded a blank matte target and a static diffuser under identical settings: within 0–15 Hz no narrowband peaks were detected (SNR < 3 dB, PLV < 0.1); experimental peaks did not coincide with typical stabilization rates (high-frequency OIS outside the analysis band; EIS updates non-periodic).

5.4 Computed observables

From ROI time series and spatial frames, the following were computed:

- power spectral density (PSD),
- two-dimensional spatial autocorrelation (2D ACF),
- temporal autocorrelation $g_2(\tau)$,
- phase-locking value (PLV),
- spatial anisotropy ΔA,
- effective correlation length L_{corr}.

5.5 Acquisition and processing parameters (summary)

Table 2: Key acquisition and processing parameters used for the reported analyses.

Parameter	**Value / range**
Laser	CW 520–532 nm; 1–5 mW on sample; spot diameter 3–8 mm; linear polarization
Optics	No diffuser; ND filter as needed (peak $\leq 70\%$ camera scale)
Geometry	Backscattering; incidence 10–20°; camera axis near normal
Distances	Laser–sample 15–30 cm; camera–sample 20–40 cm
Camera	iPhone 16 Pro Max; 1080p; 30 fps; H.264; fixed focus/exposure
Video duration	60–120 s per recording
ROI	256×256 to 512×512 px; central zone; exclude edges/glare with mask
Detrend	Enabled (1st-order)
Speckle contrast window K	11 (typical range 7–15)
Temporal smoothing	Gaussian $\sigma = 0.9$ (typical range 0.3–1.4)
PSD	0–15 Hz (at 30 fps); Welch [9]: window 1024 frames; 50% overlap; $\Delta f \approx 0.029$ Hz
2D ACF	L_{corr} from 1/e isoline; anisotropy = major/minor axis ratio at same isoline
Memory metric	Correlation of K-series across adjacent windows (2 s window, 0.5 s step); target ≥ 0.995

Reference-template alignment metrics

Template alignment was quantified using two complementary, amplitude-invariant measures: (i) a spectral-shape similarity score R and (ii) dominant-frequency phase coherence PLV_{f_0}, both evaluated against the reference fluctuation profile extracted from the aqueous reference-solution signal.

Spectral-shape similarity (R). For each ROI signal, the low-frequency PSD $P(f)$ was estimated and normalized to unit area in the comparison band: $\tilde{P}(f) = P(f) / \int_0^{3\ \mathrm{Hz}} P(f)\, df$. Spectral-template similarity was defined as the Pearson correlation coefficient

$$R = \mathrm{corr}\Big(\tilde{P}_{\mathrm{sample}}(f), \tilde{P}_{\mathrm{ref}}(f)\Big)\,.$$

Dominant-frequency phase coherence (PLV_{f_0}). The dominant low-frequency component f_0 was defined as the maximizer of $\tilde{P}_{\mathrm{ref}}(f)$ in the 0.5–2 Hz band. The sample and reference signals were band-pass filtered around f_0 (narrow-band), converted to analytic phases via the Hilbert transform, and phase-locking was computed as

$$\mathrm{PLV}_{f_0} = \Big|\Big\langle e^{i(\varphi_{\mathrm{sample}}(t) - \varphi_{\mathrm{ref}}(t))} \Big\rangle_t\Big|\,.$$

Reference-segment selection (pre-specified). The reference segment was pre-specified: the first L seconds of the reference recording (alternatively, a random length-L segment with a fixed seed); no correlation-maximizing selection was used.

Surrogates and accidental-similarity thresholds. Accidental similarity was estimated using surrogate comparisons [10, 11]: time-shuffled surrogates for R and phase-permutation surrogates for PLV_{f_0}. Thresholds are reported as the 95th percentile of the corresponding surrogate distributions (Appendix A).

6 Results

6.1 Spatial Correlations

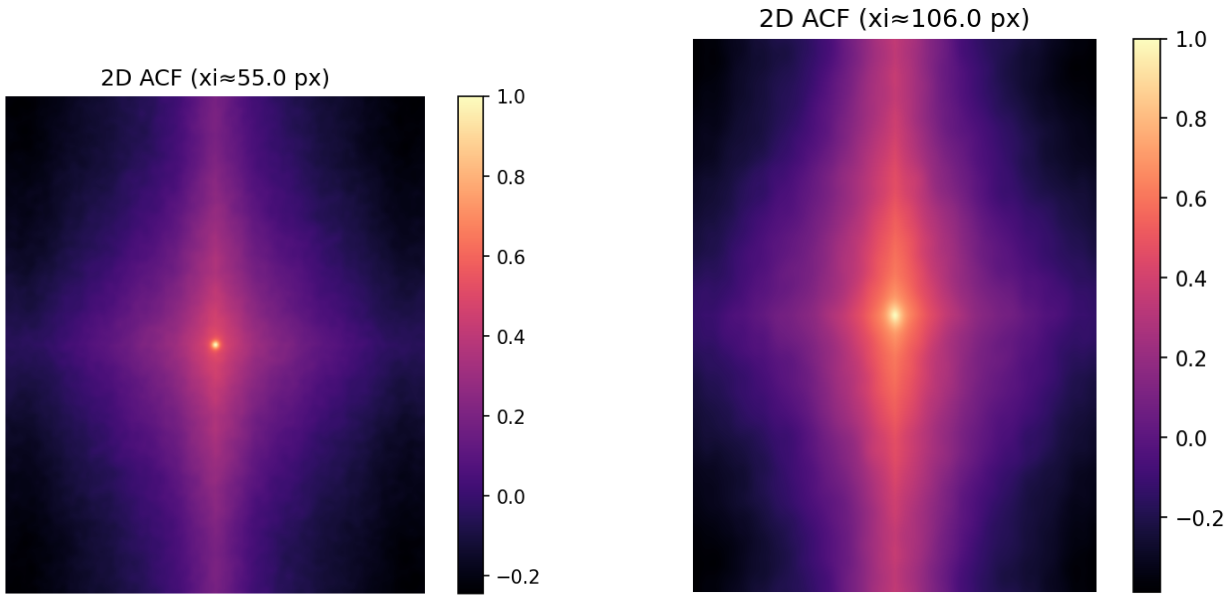

Figure 3: Two-dimensional spatial autocorrelation (2D ACF) of speckle intensity fields. The structured condition exhibits an expanded and more isotropic correlation domain compared to the chemically identical control, indicating enhanced spatial coherence under identical acquisition and processing parameters.

6.2 Spectral Characteristics

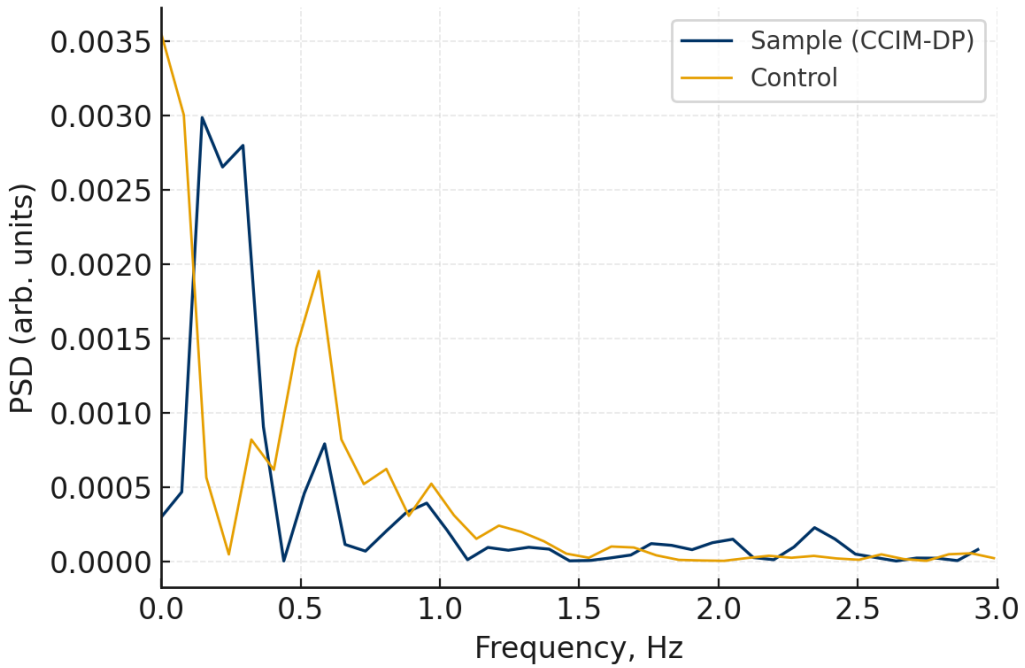

Figure 4: Power spectral density (PSD) of speckle intensity fluctuations in the low-frequency band. The structured condition shows a reproducible spectral component that is absent in the chemically identical control under identical acquisition and processing conditions.

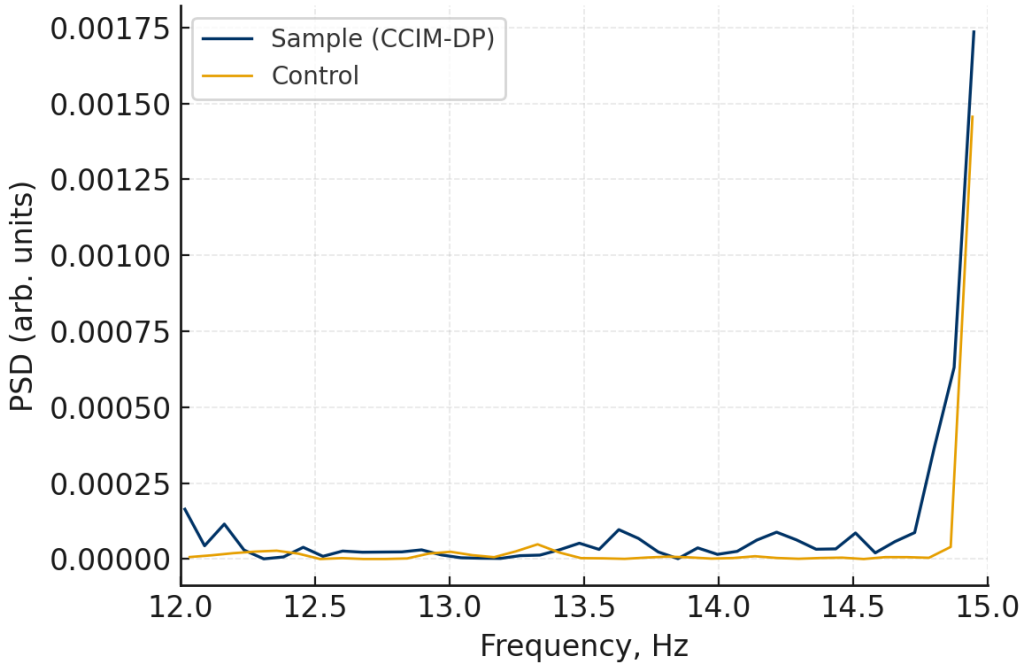

Figure 5: Power spectral density (PSD) in the higher-frequency band highlighting a narrow-band component observed in the structured condition relative to the control, computed using the same analysis pipeline.

6.3 Statistical alignment with a reference fluctuation profile

Template specificity was evaluated by comparing the structured-condition dynamics with a reference fluctuation profile extracted from optical speckle measurements of an aqueous reference solution (semaglutide; Sec. 4.2). The reference is used strictly as a physically stable fluctuation template and does not imply any biological, pharmacological, or therapeutic equivalence.

Because the reference signal may differ in acquisition duration and processing pipeline from the PSD figures shown above, it is not directly overlaid on those PSD plots. Instead, template alignment is quantified using amplitude-invariant statistical measures: normalized spectral-shape similarity and dominant-frequency phase coherence.

Using the normalized PSD-shape correlation coefficient defined in Methods, the structured CCIM-DP condition exhibits high similarity to the reference template,

$$R_{\text{structured}} = 0.96,$$

whereas the chemically identical control shows a lower similarity,

$$R_{\text{control}} \approx 0.88.$$

The dominant low-frequency component of the reference template is found at

$$f_0 \approx 0.63 \text{ Hz}.$$

Phase coherence at this component yields

$$\text{PLV}_{f_0}^{\text{structured}} \approx 0.79, \qquad \text{PLV}_{f_0}^{\text{control}} \approx 0.38.$$

Surrogate testing confirms that the structured-condition values exceed accidental-similarity thresholds, whereas the control values are consistent with weak or incidental alignment (Appendix A). Together, these results quantify selective alignment of the structured material's low-frequency fluctuation statistics with the prescribed reference template.

Replication and robustness within the present study

The reported signatures of the structured condition were observed consistently across all analyzed physical specimens ($n = 3$ per condition), multiple recordings per specimen, and multiple ROIs per recording. While figures display representative examples for visual clarity, all distributions and thresholds reported in Appendix A aggregate across the full analyzed set and use objective exclusion criteria for motion and stabilization artifacts.

7 Discussion and scope

What is new relative to existing work

Speckle-based methods are widely used to probe dynamics in soft and complex media [7]. The present work differs in that it compares specimens of identical chemical composition prepared from the same batch, differing only by a non-chemical conditioning step, and quantifies that the resulting dynamical correlation signatures can be selectively aligned with a prescribed fluctuation-statistics template. This constitutes a first experimental report of deliberate correlation-structure targeting in a condensed soft material without material transfer.

Statistical observables as projections of the model

Although the Kuramoto order parameter $r(t)$ is not directly measured, several observables act as projections of its evolution. An increase and stabilization of effective coherence is expected to manifest as: (i) emergence of narrow-band components in the PSD, (ii) elevated phase coherence measures (PLV), (iii) expanded spatial correlation length L_{corr} and reduced anisotropy in the 2D ACF, and (iv) high temporal memory across adjacent windows.

Table 3: Phenomenological mapping between Kuramoto-type dynamics and measured observables.

Kuramoto-level description	**Experimental observable**
Growth of effective coherence ($r(t) \uparrow$)	Increase of PLV; stabilization of PSD peaks
Partial synchronization	Narrow-band low-frequency component in PSD
Coherent domain formation	Increased L_{corr}; reduced anisotropy
Quasi-stationary plateau	High memory metric; reproducibility across ROIs/recordings

Time scales of correlation-order formation (two-stage kinetics)

The observed emergence of stable spectral components and expanded correlation domains is consistent with a two-stage kinetics common in non-equilibrium pattern formation and slow-relaxing soft media [1]: (i) a *nucleation/seed formation* stage (minutes to tens of minutes), followed by (ii) an *autonomous growth and stabilization* stage (hours to day-scale), during which correlation domains expand and become robust under routine handling.

Within a Kuramoto-type viewpoint, this phenomenology can be interpreted as the temporal evolution of an effective synchronization order parameter. During an initial nucleation stage (t_1), $r(t)$ increases from near-zero values as a minimal correlated seed forms. During a subsequent stabilization stage (t_2), $r(t)$ approaches a quasi-stationary plateau corresponding to a stable correlation-structured state. This interpretation is used only as a compact physical explanation of the empirically observed minutes-to-hours maturation window under fixed environmental constraints, without reliance on any disclosure of the active-step implementation.

Interpretation of semaglutide-referenced alignment and generality

The observed alignment with the semaglutide-derived reference profile should be interpreted strictly as a physical correspondence between fluctuation templates, not as any biological, pharmacological, or therapeutic equivalence. This result demonstrates that correlation order can be selectively addressed and stabilized in a condensed medium using a chosen fluctuation template. The approach is general and not limited to semaglutide or to any specific chemical system.

Limitations and outlook

As a first experimental report, the present study is limited in scope. The number of analyzed specimens is modest, and all measurements were performed using a single optical acquisition setup. Future work will extend replication across larger batches, independent acquisition systems, and external laboratories, and will explore the dependence of the observed correlation signatures on conditioning parameters, material composition, and long-term stability.

Broader relevance for correlation-engineered soft matter

Beyond the specific wax-based demonstration, the key technical result is a reproducible workflow for targeting and validating correlation-structured dynamical states using (i) a measurable reference fluctuation template, (ii) chemically identical controls, and (iii) a fixed speckle-statistics pipeline with objective artifact controls. This establishes a general experimental route toward correlation-engineered soft materials in which dynamical correlation structure can be treated as a controllable design variable rather than a by-product of composition.

8 Reproducibility and falsifiability

All optical recordings, preprocessing steps, and analysis procedures (PSD estimation, PLV_{f_0}, and surrogate testing) are fully specified and can be independently reproduced using standard imaging equipment and signal-processing libraries. The reference window length, frequency bands of interest, and similarity metrics are fixed *a priori*. Statistical significance is assessed exclusively via surrogate data generated under identical constraints.

Failure to exceed surrogate-based thresholds for R and PLV_{f_0} constitutes a negative result and falsifies the presence of structured phase alignment under the stated conditions.

9 Conclusion

We report a reproducible difference in time-resolved speckle statistics between structured and non-structured specimens drawn from the same wax-based material batch, observed across multiple physical specimens and recordings under fixed acquisition conditions. These results support the

feasibility of correlation-engineered materials characterized by reproducible, instrumentally measurable correlation dynamics and motivate a broader experimental program aimed at mapping parameter space, establishing inter-laboratory replication, and exploring generality across material classes.

Author Contributions

T.M. conceived and designed the study, performed all experiments, carried out the data analysis, and wrote the manuscript.

Competing interests

The author is affiliated with Qufit B.V. This affiliation had no influence on data acquisition, analysis, or interpretation. No external funding was received for this study.

Data and code availability

Processed data and analysis scripts supporting the findings of this study are available from the author upon reasonable request. Raw recordings are retained to ensure data integrity and verification of reported results.

Acknowledgements

The author thanks Vladimir Gorodnichii, PhD (Engineering), for conceptual discussions related to correlation-based descriptions of matter, and Gleb Meshkov for assistance with software tooling used during exploratory data analysis.

A Distributions and surrogate thresholds for R and PLV_{f_0}

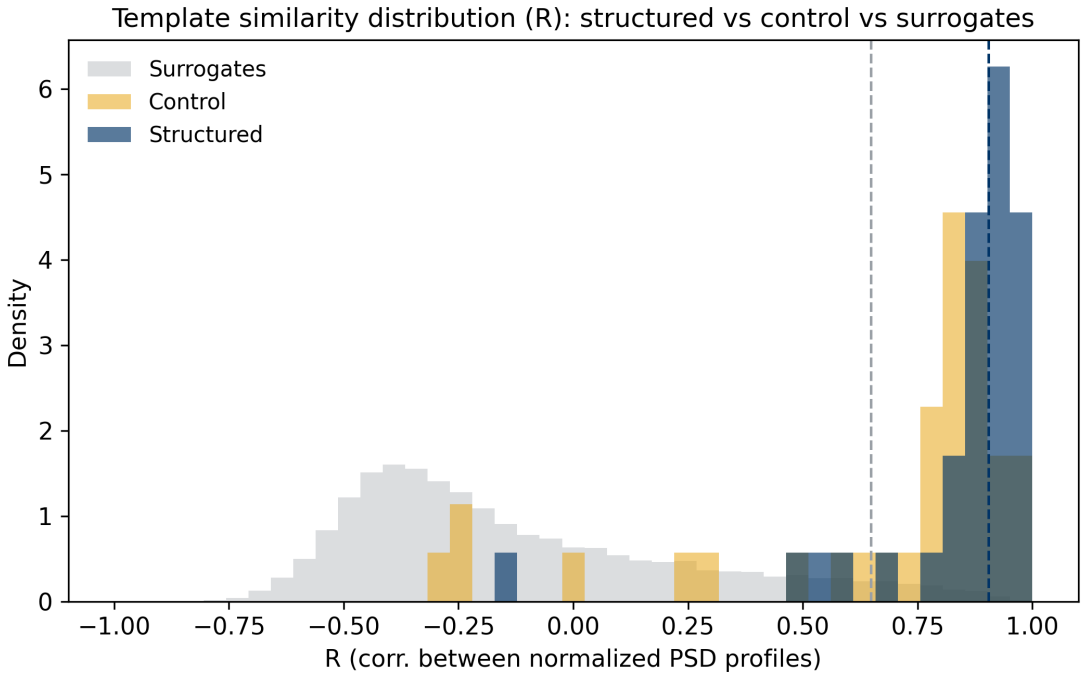

Figure 6: Distribution of the phase-locking value at the dominant reference frequency PLV_{f_0} across all analyzed regions of interest, recordings, and specimens for the structured condition, control condition, and surrogate comparisons, indicating selective phase alignment in the structured condition.

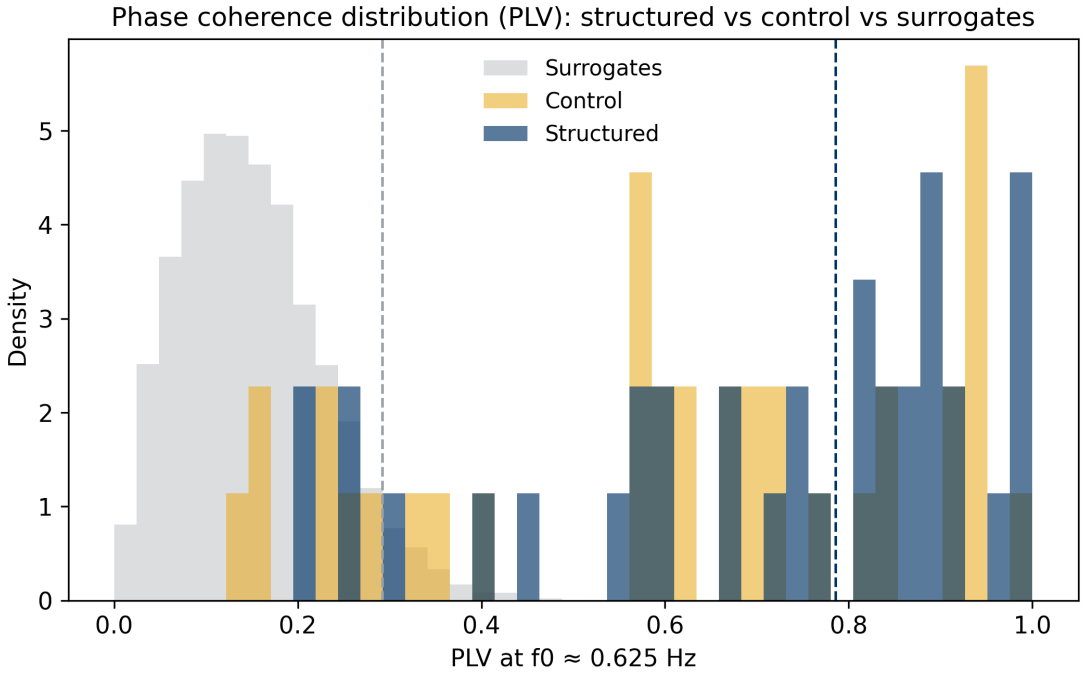

Figure 7: Distribution of the phase-locking value at the dominant reference frequency PLV_{f_0} cross all analyzed regions of interest, recordings, and specimens for the structured condition, control condition, and surrogate comparisons, indicating selective phase alignment in the structured condition.

B Phenomenological time-scale ranges (two-stage picture)

A minimal two-stage phenomenology is:

- **Stage 1 (nucleation):** formation of a minimal correlation-structured seed; characteristic time t_1.
- **Stage 2 (growth/stabilization):** expansion and stabilization of correlation domains; characteristic time t_2.

Table 4: Representative time-scale ranges used as phenomenological interpretation (orders of magnitude; not a disclosure of the active-step implementation).

Class of medium (qualitative)	t_1	t_2
High-plasticity soft media (polymer-like)	10–30 min	4–12 h
Slow-relaxing soft solids (glass-like)	40–60 min	15–20 h
Mesoscopically ordered soft systems (LC-like)	10–20 min	4–8 h

Legal Neutrality Statement

This work concerns physical correlation dynamics in condensed matter and does not imply biological, pharmacological, or therapeutic function.

References

[1] M. C. Cross and P. C. Hohenberg, "Pattern formation outside of equilibrium," *Reviews of Modern Physics* **65**, 851–1112 (1993). doi:10.1103/RevModPhys.65.851.

[2] R. Kubo, "The fluctuation–dissipation theorem," *Reports on Progress in Physics* **29**, 255–284 (1966). doi:10.1088/0034-4885/29/1/306.

[3] T. Oka and S. Kitamura, "Floquet Engineering of Quantum Materials," *Annual Review of Condensed Matter Physics* **10**, 387–408 (2019). doi:10.1146/annurev-conmatphys-031218-013423.

[4] Y. Kuramoto, *Chemical Oscillations, Waves, and Turbulence*, Springer (1984). doi:10.1007/978-3-642-69689-3.

[5] A. Pikovsky, M. Rosenblum, and J. Kurths, *Synchronization: A Universal Concept in Nonlinear Sciences*, Cambridge University Press (2001). doi:10.1017/CBO9780511755743.

[6] H. Fröhlich, "Long-Range Coherence and Energy Storage in Biological Systems," *International Journal of Quantum Chemistry* **2**, 641–649 (1968). doi:10.1002/qua.560020505.

[7] J. W. Goodman, *Speckle Phenomena in Optics: Theory and Applications* (2nd ed.), SPIE Press (2020). doi:10.1117/3.2548484.

[8] L. Mandel and E. Wolf, *Optical Coherence and Quantum Optics*, Cambridge University Press (1995). doi:10.1017/CBO9781139644105.

[9] P. D. Welch, "The use of fast Fourier transform for the estimation of power spectra," *IEEE Transactions on Audio and Electroacoustics* **15**(2), 70–73 (1967). doi:10.1109/TAU.1967.1161901.

[10] J. Theiler, S. Eubank, A. Longtin, B. Galdrikian, and J. D. Farmer, "Testing for nonlinearity in time series: the method of surrogate data," *Physica D* **58**, 77–94 (1992). doi:10.1016/0167-2789(92)90102-S.

[11] T. Schreiber and A. Schmitz, "Surrogate time series," *Physica D* **142**, 346–382 (2000). doi:10.1016/S0167-2789(00)00043-9.